Article

2D Multinuclear NMR, Hyperpolarized Xenon and Gas Storage in Organosilica Nanochannels with Crystalline Order in the Walls

Angiolina Comotti, Silvia Bracco, Patrizia Valsesia, Lisa Ferretti, and Piero Sozzani

J. Am. Chem. Soc., **2007**, 129 (27), 8566-8576• DOI: 10.1021/ja071348y • Publication Date (Web): 19 June 2007

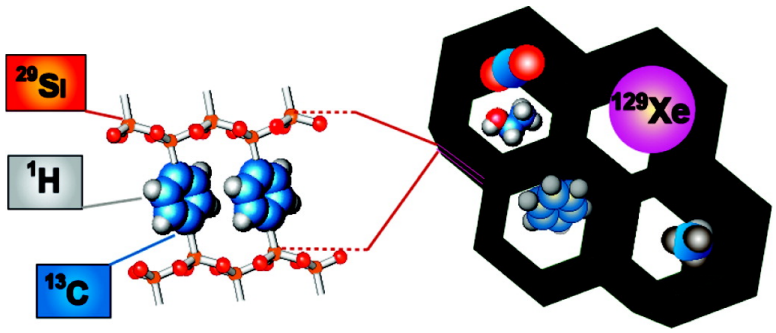

More About This Article

Additional resources and features associated with this article are available within the HTML version:

- Supporting Information
- Links to the 2 articles that cite this article, as of the time of this article download
- Access to high resolution figures
- Links to articles and content related to this article
- Copyright permission to reproduce figures and/or text from this article

View the Full Text HTML

J|A|C|S
ARTICLES
Published on Web 06/19/2007

2D Multinuclear NMR, Hyperpolarized Xenon and Gas Storage in Organosilica Nanochannels with Crystalline Order in the Walls

Angiolina Comotti, Silvia Bracco, Patrizia Valsesia, Lisa Ferretti, and Piero Sozzani*

Contribution from the Department of Materials Science and INSTM, University of Milano Bicocca, Via R. Cozzi 53, I-20125 Milan, Italy

Received February 26, 2007; E-mail: piero.sozzani@mater.unimib.it

Abstract: The combination of 2D $^{1}H-^{13}C$ and $^{1}H-^{29}Si$ solid state NMR, hyperpolarized ^{129}Xe NMR, synchrotron X-ray diffraction, together with adsorption measurements of vapors and gases for environmental and energetic relevance, was used to investigate the structure and the properties of periodic mesoporous hybrid *p*-phenylenesilica endowed with crystalline order in the walls. The interplay of ^{1}H, ^{13}C, and ^{29}Si in the 2D heteronuclear correlation NMR measurements, together with the application of Lee−Goldburg homonuclear decoupling, revealed the spatial relationships (<5 Å) among various spin-active nuclei of the framework. Indeed, the through-space correlations in the 2D experiments evidenced, for the first time, the interfaces of the matrix walls with guest molecules confined in the nanochannels. Organic−inorganic and organic−organic heterogeneous interfaces between the matrix and the guests were identified. The open-pore structure and the easy accessibility of the nanochannels to the gas phase have been demonstrated by highly sensitive hyperpolarized (HP) xenon NMR, under extreme xenon dilution. Two-dimensional exchange experiments showed the exchange time to be as short as 2 ms. Through variable-temperature HP ^{129}Xe NMR experiments we were able to achieve an unprecedented description of the nanochannel space and surface, a physisorption energy of 13.9 kJ mol^{-1}, and the chemical shift value of xenon probing the internal surfaces. These results prompted us to measure the high storage capacity of the matrix towards benzene, hexafluorobenzene, ethanol, and carbon dioxide. Both host−guest, CH$\cdots\pi$, and OH$\cdots\pi$ interactions contribute to the stabilization of the aromatic guests (benzene and hexafluorobenzene) on the extended surfaces. The full carbon dioxide loading in the channels could be detected by synchrotron radiation X-ray diffraction experiments. The selective adsorption of carbon dioxide (ca. 90 wt %) vs that of oxygen and hydrogen, together with the permanent porosity, high thermal stability, and high degree of order, makes this a suitable matrix for purifying hydrogen in clean-energy generation.

Introduction

Periodic mesoporous organosilicas (PMOs) attract a great deal of interest because of their duality in the framework that reflects the hybrid nature of the channel walls.[1] Since the discovery of periodic mesoporous hybrid materials with organic groups bridging silicon atoms, several PMO examples have been reported.[2] Indeed, interest in mesoporous materials have received a novel boost, as such materials can be prepared in a fully ordered architecture.[3] Extremely promising is the controlled organization of the organic elements, which allows the properties to be tailor-made by the juxtaposition of the proper interactions. Novel materials can thus be fabricated by the self-assembly of hybrid building blocks; these blocks cooperate with the structure-directing agent and become aligned to form an organized framework.[4] In this way the walls are constituted by a crystalline arrangement and exhibit an ordered surface. The nanochannels present not only a hexagonal packing with mesoscale periodicity but also molecular order.[3] A remarkable degree of crystalline order in the walls is achieved by using aromatic or ethylene moieties in the organic bridging group; this limits the degree of freedom during the aggregation step and favors the fabrication of a robust construction. Facing the ordered organic moieties toward the channels creates internal surfaces of a hydrophobic nature, and these can actively interact with the guest molecules[2a,3,5] and be easily functionalized with organic residues and biological receptors. Thus, properties such as sensing, selective adsorption, optoelectronics, and catalysis[1] can be tailored by fine-tuning the organic vs inorganic components in the hybrid material. For this aim the structural order at the molecular level, producing

(1) (a) Hatton, B.; Landskron, K.; Perovic, D.; Ozin, G. A. *Acc. Chem. Res.* **2005**, *38*, 305−312. (b) Hoffmann, F.; Cornelius, M.; Morell, J.; Fröba, M. *Angew. Chem., Int. Ed.* **2006**, *45*, 3216−3251.
(2) (a) Asefa, T.; MacLachlan, M. J.; Coombs, N.; Ozin, G. A. *Nature* **1999**, *402*, 867−871. (b) Inagaki, S.; Guan, S.; Fukushima, Y.; Ohsuna, T.; Terasaki, O. *J. Am. Chem. Soc.* **1999**, *121*, 9611−9614. (c) Melde, B. J.; Holland, B. T.; Blandford, C. F.; Stein, A. *Chem. Mater.* **1999**, *11*, 3302−3308.
(3) (a) Inagaki, S.; Guan, S.; Ohsuna, T.; Terasaki, O. *Nature* **2002**, *416*, 304−307. (b) Kapoor, M. P.; Yang, Q.; Inagaki, S. *J. Am. Chem. Soc.* **2002**, *124*, 15176−15177. (c) Sayari, A.; Wang, W. *J. Am. Chem. Soc.* **2005**, *127*, 12194−12195. (d) Xia, Y. D.; Wang, W. X.; Mokaya, R. *J. Am. Chem. Soc.* **2005**, *127*, 790−798.
(4) Kapoor, M. P.; Inagaki, S.; Ikeda, S.; Kakiuchi, K.; Suda, M.; Shimada, T. *J. Am. Chem. Soc.* **2005**, *127*, 8174−8178.
(5) Asefa, T.; Kruk, M.; MacLachlan, M. J.; Coombs, N.; Grondey, H.; Jaroniec, M.; Ozin, G. A. *J. Am. Chem. Soc.* **2001**, *123*, 8520−8530.

10.1021/ja071348y CCC: $37.00

highly controlled internal surfaces and virtually defect-free crystalline walls, can give an added value. Prior to this discovery, partial coverage of inorganic nanochannel walls with organic groups was obtained in a second-step process after the templating synthesis[1b] or by the incorporation of functional groups in the precursor, but no molecular order on the walls was achieved. Very recently it became possible to coerce acidic and basic groups to coexist in an organosilica.[6]

Hybrid mesoporous materials that combine both the character of crystalline nature, such as metalloorganic[7] and organic supramolecular frameworks,[8] and mesoporosity[9] provide controlled interfaces that are not yet fully understood. In fact, little is known of the relationships between organic and inorganic moieties in the highly ordered hybrid materials, or the interface interaction of the receptors facing the channels and the topology of these groups toward the channels. In addition, there has never been any exploration of the channel accessibility and storage properties of relevant vapors and gases such as methane and carbon dioxide. However, interactions at the nanochannel wall interface of hybrid mesoporous materials with guest species, and the adsorption properties of such materials, are of great interest from both the fundamental and applicative points of view. Indeed, the nature of the walls is important for the immobilization and confinement of catalysts, reactive molecules, and enzymes as well as for chromatography and separation by chemisorption or physisorption on the extended surfaces.[10] This issue is even more intriguing when organic surfaces alternate regularly with the inorganic ones, as in PMOs with crystalline-like walls where a high degree of structural control can modulate the adsorptive and storage properties as well as channel accessibility.

We used multinuclear solid-state NMR, hyperpolarized ^{129}Xe NMR, synchrotron X-ray diffraction, together with adsorption measurements of vapors and gases of environmental and energetic relevance, to investigate the structure and properties of periodic mesoporous hybrid *p*-phenylenesilica which is endowed with crystalline wall order. We exploited the most advanced solid-state and gas-phase NMR techniques to define the nanochannel space and the nanostructured interfaces as these properties are of vital importance for the tailoring of new adsorption and separation properties. Two-dimensional (2D) solid-state NMR spectroscopy, including ^{1}H−^{13}C and ^{1}H−^{29}Si Lee−Goldburg experiments,[11] can reveal the arrangement of the hybrid structures and interfaces. A deutero-organosilica matrix simplified the hydrogen spin system, and thus emphasized the host−guest interface, allowing us to unambiguously identify the molecular species of the host exposed to the channels. Using the advanced spectroscopy of hyperpolarized ^{129}Xe gas,[12] we were able to address the gas−surface affinity and the accessibility of the nanochannels, and demonstrate the suitability of the engineered channels for gas storage. For the first time, adsorption measurements were able to highlight the storage capacity and selectivity of important gases and vapors. Direct evidence of the high amount of gas stored in the porous structure was highlighted by synchrotron X-ray powder diffraction experiments.

Experimental Section

Preparation of the Mesoporous Silica Materials and the Nanocomposite. *p*-Phenylenesilica and d_4-*p*-phenylenesilica were prepared with a template synthesis where the organic−inorganic building blocks, 1,4-bis(triethoxysilyl)benzene (BTEB) and d_4-1,4-bis(triethoxysilyl)-benzene (d_4-BTEB) self-organize around amphiphilic molecules of octadecyltrimethylammonium bromide (ODTMA) in a sodium hydroxide (NaOH) aqueous solution. The molar ratios of the reactants are the following: 0.96:1.00:4.03:559.23 C_{18}TMABr/BTEB/NaOH/H_2O (or C_{18}TMABr/d_4-BTEB/NaOH/H_2O).[3] ODTMA was dissolved in the sodium hydroxide aqueous solution at 60−70 °C to ensure the complete dissolution, and then BTEB (or d_4-BTEB) was added dropwise to the solution under vigorous stirring at room temperature. The mixtures were treated ultrasonically for 20 min to improve dispersion, stirred at room temperature for 20 h, and then kept at 95 °C for 20 h under static conditions. The white precipitates were recovered by filtration and dried to yield the *p*-phenylenesilica and d_4-*p*-phenylenesilica materials containing the surfactant molecules (hereafter called nanocomposites). The surfactant was washed away by stirring 1 g of powder in 250 mL of ethanol and 9 g of 36% hydrochloride aqueous solution at 70 °C for 8 h, thus producing the mesoporous materials.

Synthesis of d_4-1,4-Bis(triethoxysilyl)benzene. d_4-1,4-Bis(triethoxysilyl)benzene was prepared via a Grignard reaction on the *p*-dibromo precursor. Magnesium and tetraethoxysilane (TEOS) were mixed in tetrahydrofuran (THF) under nitrogen with a catalytic amount of iodine and brought to reflux. The reactant molar ratios used are the following: 0.62 Mg/2.00 TEOS/0.20 dibromobenzene. A solution of d_4-1,4-dibromobenzene in THF was added dropwise in 2 h to the reaction vessel, and the final mixture was refluxed for 2 h. The gray-green mixture was cooled, and THF was removed under vacuum. Hexane was added to extract the product from the remaining magnesium salts. After filtration, the hexane was removed under vacuum, leaving a brown oil, which was distilled yielding the d_4-BTEB clear colorless oil. ^{1}H NMR ($CDCl_3$, 400 MHz) of d_4-BTEB: δ 3.89 (q, 2H), 3.87 (q, 2H), 3.85 (q, 2H), 3.83 (q, 2H), 1.26 (t, 3H), 1.24 (t, 3H), 1.22 (t, 3H). ^{13}C NMR ($CDCl_3$, 100.7 MHz) of d_4-BTEB CD: δ t, 133.37, 133.12 and

(6) (a) Alauzun, J.; Mehdi, A.; Reye, C.; Corriu, R. J. P. *J. Am. Chem. Soc.* **2006**, *128*, 8718−8719. (b) Jaroniec, M. *Nature* **2006**, *442*, 638−640.
(7) (a) Kitagawa, S.; Kitaura, R.; Noro, S. *Angew. Chem., Int. Ed.* **2004**, *43*, 2334−2375. (b) Ockwig, N. W.; Delgado-Friedrichs, O.; O'Keeffe, M.; Yaghi, O. M. *Acc. Chem. Res.* **2005**, *38*, 176−182. (c) Bradshaw, D.; Claridge, J. B.; Cussen, E. J.; Prior, T. J.; Rosseinsky, M. J. *Acc. Chem. Res.* **2005**, *38*, 273−282.
(8) (a) Atwood, J. L.; Steed, J. W. *Supramolecular Chemistry*; Wiley: Weinheim, 2000. (b) Ward, M. D. *Chem. Commun.* **2005**, 5838−5842. (c) Sozzani, P.; Bracco, S.; Comotti, A.; Ferretti, L.; Simonutti, R. *Angew. Chem., Int. Ed.* **2005**, *44*, 1816−1820. (d) Malek, N.; Maris, T.; Perron, M. P.; Wuest, J. D. *Angew. Chem., Int. Ed.* **2005**, *44*, 4021−4025. (e) Nangia, A. *Curr. Opin. Solid State Mater. Sci.* **2001**, *5*, 115−122. (f) Gorbitz, C. H. *Chem. Eur. J.* **2001**, *7*, 5153−5159.
(9) (a) Kresge, C. T.; Leonowicz, M. E.; Roth, W. J.; Vartuli, J. C.; Beck, J. S. *Nature* **1992**, *359*, 710 − 712. (b) Yang, P. D.; Zhao, D. Y.; Margolese, D. I.; Chmelka, B. F.; Stucky, G. D. *Nature* **1998**, *396*, 152−155. (c) Sakamoto, Y.; Kaneda, M.; Terasaki, O.; Zhao, D. Y.; Kim, J. M.; Stucky, G.; Shin, H. J.; Ryoo, R. *Nature* **2000**, *408*, 449−453. (d) Joo, S. H.; Choi, S. J.; Oh, I.; Kwak, J.; Liu, Z.; Terasaki, O.; Ryoo, R.; Zou, X.; Conradsson, T.; Klingstedt, M.; Dadachov, M. S. *Nature* **2001**, *412*, 169−172. (e) Zou, X.; Conradsson, T.; Klingstedt, M.; Dadachov, M. S.; O'Keeffe, M. *Nature* **2005**, *437*, 716 − 719. (f) Sozzani, P.; Bracco, S.; Comotti, A.; Simonutti, R.; Valsesia, P.; Sakamoto, Y.; Terasaki, O. *Nat. Mater.* **2006**, *5*, 545−551.
(10) (a) Ozin, G. A.; Arsenault, A. C. *Nanochemistry*; Royal Society of Chemistry Publishing: Cambridge, 2005. (b) Fukuoka, A.; Sakamoto, Y.; Guan, S.; Inagaki, S.; Sugimoto, N.; Fukushima, Y.; Hirahara, K.; Iijima, S.; Ichikawa, M. *J. Am. Chem. Soc.* **2001**, *123*, 3373−3374. (c) Rebbin, V.; Schmidt, R.; Fröba, M. *Angew. Chem., Int. Ed.* **2006**, *45*, 5210−5214.
(11) (a) Vinagradov, E.; Madhu, P. K.; Vega, S. *Chem. Phys. Lett.* **1999**, *314*, 443−450. (b) Van Rossum, B. J.; De Groot, C. P.; Ladizhansky, V.; Vega, S.; De Groot, H. J. M. *J. Am. Chem. Soc.* **2000**, *122*, 3465−3472. (c) Sozzani, P.; Bracco, S.; Comotti, A.; Camurati, I.; Simonutti, R. *J. Am. Chem. Soc.* **2003**, *125*, 12881−12893. (d) Sozzani, P.; Comotti, A.; Bracco, S.; Simonutti, R. *Chem. Commun.* **2004**, 768−769. (e) Sozzani, P.; Comotti, A.; Bracco, S.; Simonutti, R. *Angew. Chem., Int. Ed.* **2004**, *43*, 2792−2797.
(12) (a) Long, H. W.; Gaede, H. C.; Shore, J.; Reven, L.; Bowers, C. R.; Kritzenberger, J.; Pietrass, T.; Pines, A.; Tang, P.; Reimer, J. A. *J. Am. Chem. Soc.* **1993**, *115*, 8491−8492. (b) Haake, M.; Pines, A.; Reimer, J. A.; Seydoux, R. *J. Am. Chem. Soc.* **1997**, *119*, 11711−11712. (c) Brunner, E.; Haake, M.; Pines, A.; Reimer, J. A.; Seydoux, R. *Chem. Phys. Lett.* **1998**, *290*, 112−116. (d) Seydoux, R.; Pines, A.; Haake, M.; Reimer, J. A. *J. Phys Chem. B* **1999**, *103*, 4629−4637.

132.88 ppm, C−Si: δ s, 132.40 ppm. For comparison the ^{13}C NMR ($CDCl_3$, 400 MHz) of BTEB are reported: CH s, 134.38 ppm and C−Si s, 133.43 ppm.

Solid-State NMR. The solid−state NMR spectra were run at 75.5 MHz for ^{13}C and 59.6 MHz for ^{29}Si, on a Bruker Avance 300 instrument operating at a static field of 7.04 T equipped with 4 mm double resonance MAS probe. The samples were spun at the magic angle at a spinning speed of 15 kHz, and ramped-amplitude cross-polarization (RAMP-CP) transfer of magnetization was applied. The 90° pulse for proton was 2.9 μs. ^{13}C Single-pulse excitation (SPE) experiments were run using a recycle delay of 100 s and cross polarization (CP) MAS experiments were performed using a recycle delay of 10 s and contact times of 2 and 8 ms. Quantitative ^{29}Si SPE experiments with dipolar decoupling from hydrogen were run using a recycle delay of 500 s; typical CP MAS experiments were performed using a recycle delay of 10 s and a contact time of 6 ms. ^1H MAS NMR experiment was performed with a recycle delay of 20 s.

Phase-modulated Lee−Goldburg (PMLG) heteronuclear $^1H-^{29}Si$ and $^1H-^{13}C$ correlation (HETCOR) experiments coupled with fast magic angle spinning (15 kHz) allowed the recording of 2D spectra with high-resolution both in the hydrogen, silicon, and carbon dimensions.[11] Narrow hydrogen resonances, with line widths in the order of 1−2 ppm, were obtained with homonuclear decoupling during t_1; this resolution permits a sufficiently accurate determination of the proton species present in the system. PMLG $^1H-^{29}Si$ and $^1H-^{13}C$ HETCOR spectra were run with LG period of 18.9 μs. The efficient transfer of magnetization to the carbon and silicon nuclei was performed applying RAMP-CP sequence. Quadrature detection in t_1 was achieved by time proportional phase increments method. Carbon and silicon signals were acquired during t_2 under proton decoupling applying two-pulse phase modulation scheme (TPPM).[13] Before each heteronuclear experiment samples were outgassed overnight at 160 °C and inserted in the ZrO_2 rotors in a dry box under nitrogen atmosphere.

Hyperpolarized Xe NMR. Hyperpolarization ^{129}Xe NMR experiments were performed using a homemade apparatus incorporating a continuous-flow delivery of hyperpolarized xenon gas, and measurements were made on a Bruker Avance 300 spectrometer operating at a Larmor frequency of 83.02 MHz for ^{129}Xe. A diode array laser delivering 16 W at 795 nm was applied. A stream of gas mixture containing 2% xenon, 2% nitrogen, and 96% helium was used in most of the experiments, and gas flow rates were optimized between 200−300 cm^3/min. The polarization was about 5%. The samples were pressed in pellets and outgassed overnight at 160 °C and then inserted in the coil and equilibrated in the gas stream for at least 20 min before collecting the NMR spectra.

Typically, the spectra were recorded with 128 scans and 0.5−2 s of recycle delays. Variable temperatures were achieved by flowing cooled or heated nitrogen gas around the sample region. Two-dimensional (2D) exchange NMR is a powerful technique to investigate dynamic processes occurring on a time scale up to several seconds.[14] The 2D exchange experiments were run with spectral width of 29 kHz in both t_1 and t_2 dimensions. There were 128 t_1 increments; 2D data were collected in TPPI mode. Mixing times were varied from 1 to 30 ms. The ^{129}Xe NMR chemical shifts were referenced to xenon gas extrapolated to zero pressure.

Synchrotron X-ray Powder Diffraction. Synchrotron X-ray powder diffraction experiments were performed at the European Synchrotron Radiation Facility (ESRF) in Grenoble on the BeamLine D8, with a Debye−Scherrer type diffractometer equipped with a gas handling system. The radiation wavelength λ of the incident X-rays was 0.78 Å; 2θ range was from 2° to 35°. The powder sample was loaded into a glass capillary, inner diameter 0.8 mm. The temperature was controlled by a low-temperature nitrogen gas blower. The sample was heated at 160 °C for 3 h in vacuum to remove residual water molecules present in the nanochannels. The experiments on the mesoporous material were performed at variable temperature, at rt to 200 K. The diffraction patterns of the carbon dioxide loaded sample were performed at different temperatures under 1 atm constant pressure; the carbon dioxide gas was flowed into the capillary sample through a stainless steel tube. Once the equilibrium adsorption state was reached, the sample was left exposed to the gas for 2 h before acquiring the diffraction patterns.

Transmission Electron Microscopy. The TEM images were obtained using a JEOL JEM-3010 with $V = 300$ kV. Laser light diffraction analyses were performed using Tri-laser Microtrac S3500 apparatus.

Volumetric Adsorption Measurements. Nitrogen adsorption−desorption isotherms were measured at liquid nitrogen temperature using a Micromeritics analyzer. The samples were outgassed overnight at 150 °C under vacuum. Surface area was calculated using the Brunauer, Emmet, and Teller (BET) model. The pore-size distributions were evaluated following the method developed by Barret, Joyner, and Halenda (BJH model) for cylindrical pores with Kruk−Jaroniec−Sayari correction, and by nonlinear density functional theory (DFT) analysis. The BJH adsorption volume of mesopores essentially equaled the total pore volume, thus excluding significant microporosity in the samples; the same conclusion was reached by DFT analysis. No hysteresis was apparent throughout the entire pressure range. The BET surface area and the pore volume of the *p*-phenylenesilica mesoporous material from nitrogen adsorption were 780.34 $m^2\ g^{-1}$ and 0.78 $cm^3\ g^{-1}$, respectively. The pore width, evaluated by DFT analysis, was 40 Å.

Benzene, hexafluorobenzene, and cyclohexane absorption isotherms were determined by volumetric measurements equipped with precision manometers (±0.5 Torr). The adsorption equilibrium was normally reached in less than 30 min. The measurements were carried out at room temperature and in a pressure range where the vapor phases behave as an ideal gas. The adsorption isotherms of ethanol were performed at 298 and 273 K and the oxygen isotherm at 273 K. The isotherms of xenon, methane, and carbon dioxide were measured at 298 and 195. The adsorption kinetics were followed for each point, and the equilibrium value was reported in the isotherms.

Results and Discussion

The hybrid mesoporous material derived from 1,4-bis-(triethoxysilyl)benzene presenting hexagonal nanochannels and crystal-like regularity in the channel walls is schematically depicted in Figure 1a. The highly ordered arrangement of the structure, on both the mesoscale and the nanoscale, is testified to by the TEM images and electron diffraction patterns that enable the molecular level resolution (Figure 2). In the electron diffraction patterns it is possible to recognize spots of the 45.7 Å periodicity due to the mesoscale hexagonal arrangement, and diffused spots of 7.6 Å due the periodicity along the channel direction.[3] The hexagonal shape of the nanochannels can be clearly seen in the TEM images. A complete set of *d*-spacing on the different scale lengths could be obtained by synchrotron X-ray powder pattern, that shows at low angles ($2\theta < 5°$ at the wavelength of 0.78 Å) the *d*-spacings of 45.74, 26.35, 22.74 Å due to the hexagonal lattice and, at higher angles, the sharp peaks of the interplanar distances at 7.55, 3.79, 2.52 Å associated to the molecular order along the channel direction. The reflection at the *d*-spacing of 4.35 Å corresponds to the repeat period on the *a*−*b* plane of the building blocks. From these data the lattice constant of the 2D hexagonal lattice on the mesoscale is $a = 52.8$ Å ($a = d^*2/3^{1/2}$). The synchrotron X-ray diffraction pattern of *p*-phenylenesilica mesoporous material (Figure 1b) presents

(13) Bennet, A. E.; Rientra, C. M.; Auger, M.; Lakshmi, K. V.; Griffin, R. G. *J. Chem. Phys.* **1995**, *103*, 6951−6958.
(14) (a) Ernst, R. R.; Bodenhausen, G.; Wokaun, A. *Principles of Nuclear Magnetic Resonance in One and Two Dimensions*; Oxford University Press: London, 1990. (b) Kritzenberger, J.; Gaede, H. C.; Shore, J.; Pines, A. *J. Phys. Chem.* **1994**, *98*, 10173−10179.

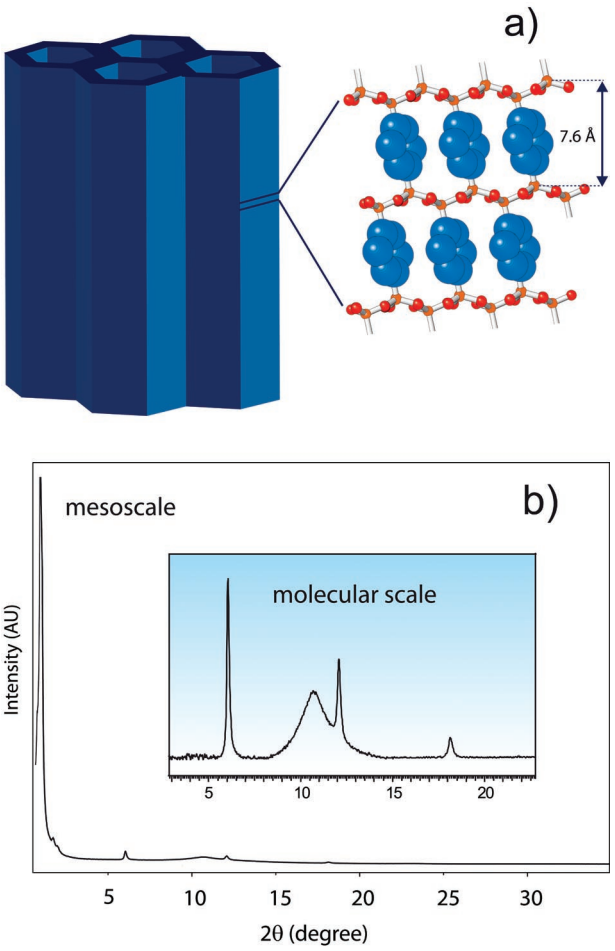

Figure 1. (a) Sketch of the mesoporous *p*-phenylenesilica architecture containing ordered arrays of hybrid building blocks in the channel walls. (b) Synchrotron radiation X-ray diffraction pattern showing the reflections on both the mesoscale and the molecular scale (the wavelength of 0.78 Å was used).

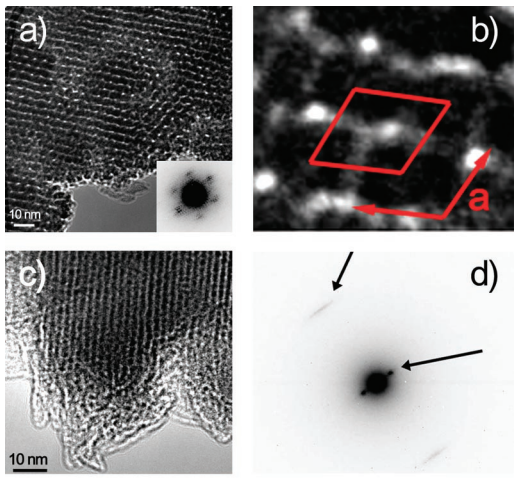

Figure 2. TEM micrographs of the hybrid mesoporous material: (a) hexagonal arrangement of the nanochannels viewed along the channel axis (the electron diffraction pattern is reported in the insert); (b) enlargement of the hexagonal arrangement of the nanochannel; (c) arrangement of the nanochannels viewed perpendicular to the channel axis; (d) electron diffraction pattern collected perpendicularly to the channel axis.

a higher signal-to-noise ratio and higher resolution than conventional X-ray diffraction experiments, and the presence of crystalline impurities in our sample was thus excluded. In

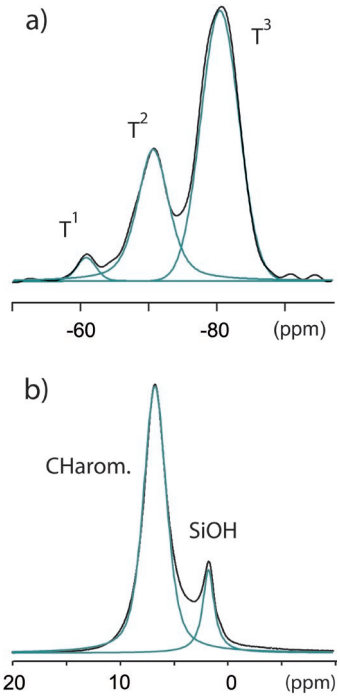

Figure 3. (a) 1D ^{29}Si MAS NMR spectrum of benzene silica performed under quantitative conditions applying a recycle delay of 500 s. The peaks are assigned to the T^n condensed species where *n* denotes the number of siloxane bonds. (b) ^{1}H MAS NMR spectrum with spinning speed of 15 kHz and 20 s of recycle delay.

principle, the very marked brightness of the X-ray source would have enabled us to recognize the presence of even small amounts of spurious crystalline phases had they been present. Further characterizations are reported in the Experimental Section and Supporting Information.

The framework consists of alternate inorganic and organic layers connected by Si−C covalent bonds. The condensation state of silyl moieties in the inorganic layer can be accurately described by solid-state MAS NMR spectroscopy exploiting the hydrogen, silicon, and carbon nuclei. The ^{29}Si MAS NMR spectrum performed with 500s of recycle delay (Figure 3a) shows resonances at −80.5, −70.4, and −60.9 ppm, associated with the silicon condensed species: the completely reacted species that represent a fully condensed silicon are called T^3, while the species containing one and two OH groups are called T^2 and T^1, respectively.[15] Our approach focused on the ^{29}Si MAS NMR spectrum to evaluate, under quantitative conditions, the content of the silicon species, and this was ensured by the long recycle delays, 5 times longer than the ^{29}Si spin−lattice relaxation times measured independently (^{29}Si T_1 relaxation times: $T^3 = 83$ s, $T^2 = 30$ s, and $T^1 = 19$ s). In this way we were able to obtain, for the first time, a reliable quantification of the amount of the condensed species, found to be 64.9%, 32.3%, and 2.8% for the T^3, T^2, and T^1 species, respectively. This represents a 2:1 ratio of T^3/T^2 species, indicating the presence of one silanol over 9 Si−O bonds. The minor amount of geminal silanols (T^1) can probably be associated to defects in the structure; apparently these defectes do not pertain to the crystal structure and are thus not detected by synchrotron X-ray diffraction as diffractometric techniques are not sensitive to local

(15) Shea, K. J.; Loy, D. A.; Webster, O. *J. Am. Chem. Soc.* **1992**, *114*, 6700−6710.

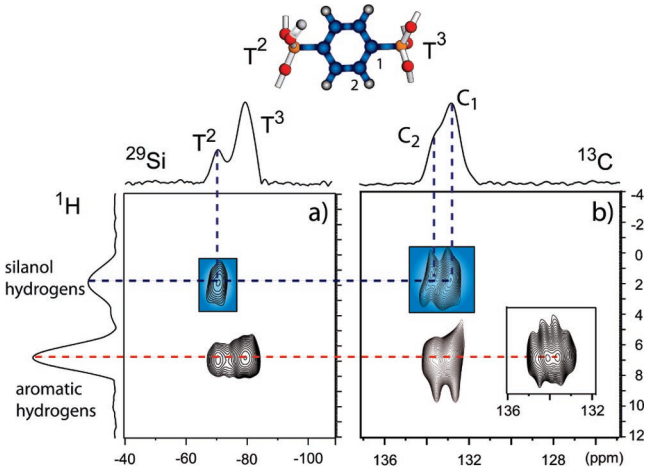

Figure 4. (a) 2D $^{1}H-^{29}Si$ and (b) 2D $^{1}H-^{13}C$ Lee−Goldburg heterocorrelated MAS NMR spectra of the mesoporous *p*-phenylenedilica performed at a spinning speed of 15 kHz and a contact time of 2 ms. (Insert) 2D $^{1}H-^{13}C$ heterocorrelated NMR spectrum at a contact time as short as 100 μs.

defects and amorphous phases. No Q species were detected due to cleavage of silicon−carbon bonds. From ^{1}H MAS NMR spectrum silanol hydrogens can be detected at 1.8 ppm, together with the aromatic hydrogens on the organic moiety at 6.8 ppm (Figure 3b). The quantitative analysis of the ^{1}H MAS spectrum revealed 1 OH group out of 6 aromatic hydrogens, confirming the 2:1 ratio for the T^3/T^2 species. Differently from purely siliceous mesoporous materials like MCM-41, the presence of aromatic hydrogens in the organosilica material provides a reference value for the quantification of OH groups in the ^{1}H spectrum. The signal at 1.8 ppm is typical of silanols of siliceous materials in the absence of hydrogen exchange with water, confirming an anhydrous sample.[16] In fact, the sample was dried carefully at 150 °C and 10^{-2} Torr overnight. Prior to the thermal treatment, the ^{1}H spectra show signals at 2.8 and 5 ppm, due to the presence of water. ^{13}C MAS NMR is less informative; two chemically different carbon atoms (C−Si and CH) are present, but their chemical shifts overlap at 133.7 ppm because of the upfield shift of the silicon on the quaternary carbon.[17]

The inorganic layer in the channel walls has been described as an array of condensed six-member rings formed by silicon tetrahedra generating a regular sequence of alternate T^3 and T^2 species.[3] The quantitative determination of T^3/T^2 condensed species, performed here in the simple stoichiometric ratio of 2:1, suggests a model where the wall of the hexagonal channel is constituted by alternate six- and four-member rings, and thus of a repeat unit of $(T^3-T^2-T^3)_n$ along each wall face, giving rise to T^3/T^2 ratio of 2.

Two-dimensional solid state NMR experiments directly measure the spin-correlations of unlike nuclei, namely $^{1}H-^{29}Si$ and $^{1}H-^{13}C$ (Figure 4). From the $^{1}H-^{29}Si$ 2D heterocorrelated NMR spectrum with homonuclear Lee−Goldburg decoupling,[11] fast magic angle spinning, and 2 ms contact time, one can observe that the silanols are correlated only with T^2 silicons to which they are connected (hydrogen-to-silicon distance of 1.8 Å). On the contrary, the aromatic hydrogens correlate with both silicon species, T^2 and T^3, since each silicon bears its own organic group and sits at the same distance ca. 3 Å from aromatic hydrogens. Interestingly, in $^{1}H-^{13}C$ 2D spectra, the silanols correlate, with almost the same intensity, with both the carbons, demonstrating that the dangling Si−OH bond explores conformations folded toward the aromatic ring. In both the 2D spectra the spin system of the building blocks bearing the T^2 groups is clearly independent (highlighted in blue in Figure 4) of that containing the T^3 condensed species. The $^{1}H-^{13}C$ heterocorrelated 2D spectrum performed at a contact time of 2 ms shows marked resolution, and this allowed us to distinguish, for the first time, the two carbon resonances that overlap in the 1D spectrum. The aromatic hydrogens, especially for contact times as short as 100 μs (insert of Figure 4), revealed two separate carbon signals at 134.3 and 133.5 ppm, and by following the dynamics of signal intensity at variable contact times we were able to assign the two chemical shifts to the protonated CH and non-protonated C−Si aromatic carbons, respectively. The presence of only two resonances confirms the highly symmetric arrangement of the *p*-phenylene group in the ordered walls. The assignment of the signals is further supported on the basis of the ^{13}C NMR spectrum in solution of the monomer deuterated on the aromatic ring, where the triplet of the CD carbon resonates downfield from that of the carbon-bearing silicon atom (see Experimental Section). In solution, the two resonances of 1,4-bis(triethoxysilyl)benzene[15] were detected, but the univocal assignment to the C−H and C−Si species was made possible by the deuteration of the aromatic ring (d_4-1,4-bis(triethoxysilyl)benzene) that generates a triplet signal for the CD coupling.

The nanocomposite material with surfactant is of interest to better understand how the walls interact with the chemical species filling the nanochannel space and to explore the interface of the hybrid mesoporous system. A deuterated matrix was prepared to highlight targeted spatial relationships at the interface between host and guests. The 1D ^{1}H MAS NMR spectrum of the d_4-*p*-phenylenesilica nanocomposite indicates the absence of the hydrogen aromatic signal, in accordance with the selective deuteration of the sample (Figure 5).

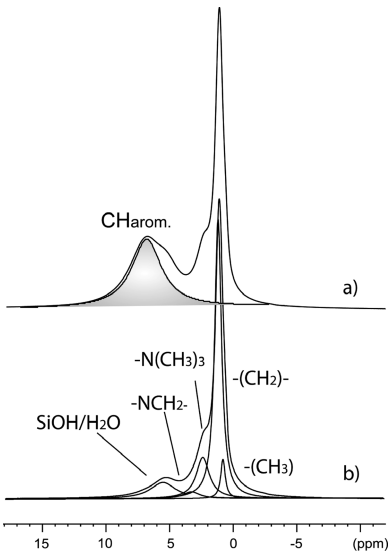

Figure 5. ^{1}H MAS NMR spectra at a spinning speed of 15 kHz and a recycle delay of 20 s of (a) *p*-phenylenesilica and (b) d_4-*p*-phenylenesilica nanocomposites containing octadecyltrimethylammonium bromide.

For comparison purposes the ^{1}H MAS NMR spectrum of the

(16) Grünberg, B.; Emmler, T.; Gedat, E.; Shenderovich, I.; Findenegg, G. H.; Limbach, H.-H.; Buntkowsky, G. *Chem. Eur. J.* **2004**, *10*, 5689−5696.
(17) Rakita, P. E.; Worsham, L. S. *J. Organomet. Chem.* **1977**, *137*, 145−155.

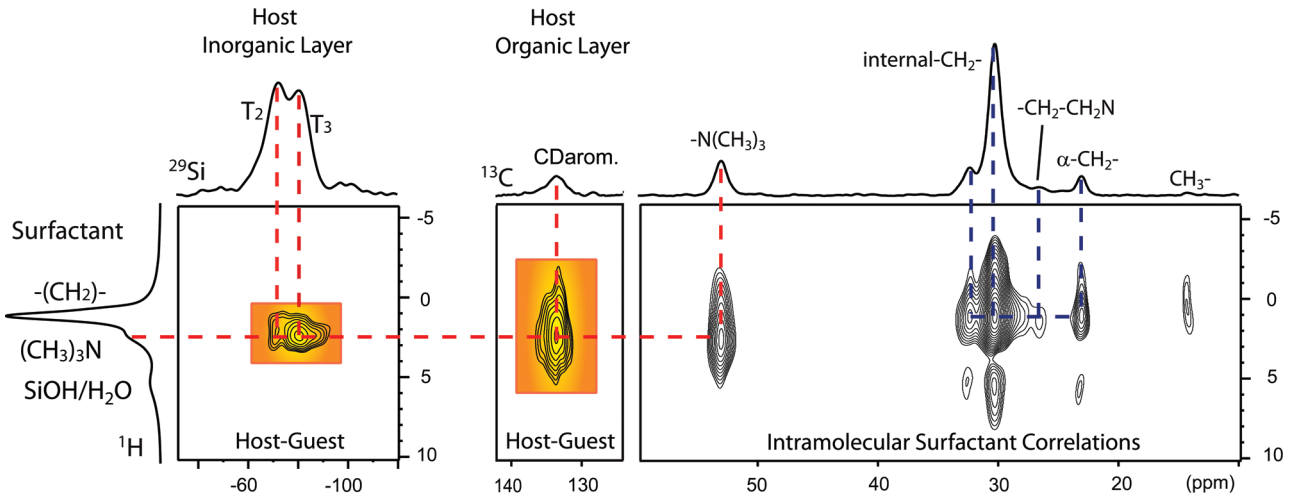

Figure 6. 2D $^{1}H-^{29}Si$ and $^{1}H-^{13}C$ Lee−Goldburg heterocorrelated NMR spectra with 8 ms contact time of the d_4-*p*-phenylenesilica nanocomposite with octadecyltrimethylammonium bromide. Inserts in orange color indicate the intermolecular organic−inorganic and organic−organic correlations of the surfactant molecules with the matrix. Dashed blue lines show the correlations of the surfactant carbons to the covalently bonded hydrogens (^{13}C projection). In the hydrogen and silicon domains the 1D ^{1}H MAS NMR and ^{29}Si CP MAS NMR spectra are reported, respectively.

fully hydrogenated sample is reported. Once the aromatic hydrogens were removed, the deuterated sample showed the signal at 5.45 ppm due to the residual presence of water.

Two-dimensional $^{1}H-^{29}Si$ heterocorrelated NMR spectra of d_4-*p*-phenylenesilica nanocomposite (Figure 6 and Supporting Information) show the hydrogen signals on the surfactant heads correlating with the T^2 and T^3 silicon species; these indicate that the condensed inorganic groups face the channels and interact with the surfactant. The space traveled by the magnetization through dipole−dipole interactions is sufficient to cross the heterogeneous organic−inorganic interfaces, depicting an intimate nanoscale system. The correlations identify the close proximity of the polar heads of the surfactant to the inorganic layer, while the long hydrocarbon tails stay apart from the surface. As a novelty feature of the organosilicas with respect to the conventional mesoporous silicas,[18] the hybrid nature of its surface allows the observation of host−guest correlations with the additional nuclei of carbon that are present in the organic moieties of the channel walls. The 2D $^{1}H-^{13}C$ heterocorrelated spectra (Figure 6 and Supporting Information) present a few cross-peaks due to intramolecular correlations of hydrogens bonded to the carbons, but most interestingly, there is a cross-peak that pertains to the intermolecular interaction of the surfactant molecules adhering to the aromatic rings on the channel walls. In fact, the methyls on the polar head $N(CH_3)_3$ of the guest $\delta_H = 2.3$ ppm correlate with the aromatic carbons of the host (Figure 6, highlighted in orange), indicating that, also for the organic layer, the prevailing interaction at the interface involves the heads of the surfactants. This can be explained by the bulkiness of the head groups that, while interacting with the silicon inorganic layers, also cover the organic moieties, not leaving enough space for the long hydrocarbon tails to access the interface (Figure 7). The correlation of the signal at $\delta_H = 2.3$ ppm with the carbon atoms at $\delta_C = 54.3$ ppm supports the assignment of these hydrogen signals to the methyls on nitrogen. To the best of our knowledge, this is the first direct observation of an intermolecular organic−organic spatial relationship in mesoporous hybrid materials.

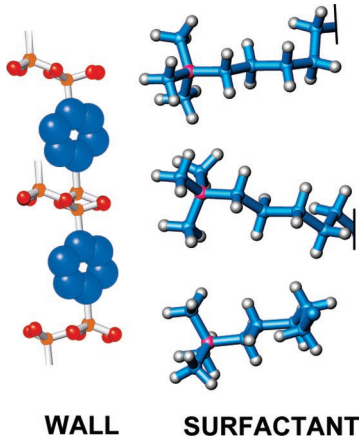

Figure 7. Structure of the nanocomposite interface showing the hybrid building blocks of the nanochannel walls interacting with the polar heads of the surfactant molecules as highlighted by $^{1}H-^{13}C$ and $^{1}H-^{29}Si$ 2D MAS NMR.

The internal methylenes of the surfactant chains, as well as the α- and *β*-methylenes, generate cross-peaks between the methylene hydrogens at $\delta_H = 1.1$ ppm and the covalently bonded carbon atoms at 30.6, 23.3, and 32.6 ppm, respectively. The most upfield cross-peak in both the hydrogen and carbon domains ($\delta_H = 0.7$ and $\delta_C = 14.4$ ppm) corresponds to the methyls on the chain-end of the surfactant molecules. From the chemical shift of the methylene chains at 30.6 ppm (inner-CH_2) and that of the chain-end methyl of the hydrocarbon tail it is clear that the chains are arranged in gauche-rich conformations.[19] The carbon relaxation times of the internal methylenes, as short as 450 ms at room temperature, correspond to maximum relaxation efficiency and a correlation time of 10 ns at the observation frequency of 75 MHz. These determinations depict a gel-like behavior of the surfactant in the confining matrix. No further signals from surfactants outside the channels in the bulk are observed. The presence of the chains exclusively within the channels is confirmed by powder X-ray diffraction experiments (Supporting Information). Because of the decrease in the electron density contrast, the powder pattern of the d_4-*p*-

(18) (a) Janicke, M. T.; Landry, C. C.; Christiansen, S. C.; Kumar, D.; Stucky, G. D.; Chmelka, B. F. *J. Am. Chem. Soc.* **1998**, *120*, 6940−6951. (b) Simonutti, R.; Comotti, A.; Bracco, S.; Sozzani, P. *Chem. Mater.* **2001**, *13*, 771−777.

(19) Bracco, S.; Comotti, A.; Simonutti, R.; Camurati, I.; Sozzani, P. *Macromolecules* **2002**, *35*, 1677−1684.

phenylenesilica nanocomposite shows a reduced intensity of the mesoscale periodicity (*d*-spacing of 4.6 nm), compared with the same peak of the mesoporous material. No peaks of crystalline surfactant are present. The amount of surfactant residing in the channels was measured by thermogravimetric analysis and quantitative ^{13}C MAS spectrum as being 29% and 27% by weight, respectively (Supporting Information). This is proof that the channels are largely occupied by the surfactant, and that the guest molecules act as a probe of the host species facing the channel.

Hyperpolarized ^{129}Xe NMR in Mesoporous *p*-Phenylenesilica. HP ^{129}Xe NMR is an advanced technique that probes the nature of the pore walls and the space available to the diffusing gases.[12] Recently, it was applied to mesoporous materials with amorphous arrangement in the channel walls.[20] The hyperpolarized technique has been applied here, for the first time, to periodic mesoporous materials endowed with a high degree of order on the molecular scale. HP ^{129}Xe NMR experiments, in the continuous flow mode, enable the detection of xenon diffused to the nanochannels of the crystal-like organosilica, in addition to the gas signal at 0 ppm (Figure 8a). The xenon resonance can be collected after a few milliseconds of xenon diffusion in the channels, and down to the limit of low concentration of 2% (see Experimental Section) and low fraction of xenon (0.02 mmol Xe/g organosilica at room temperature), that allows the exclusive observation of xenon−wall interactions, xenon−xenon interactions being virtually absent. At room temperature the chemical shift of the adsorbed xenon falls at 92 ppm, indicating a typical chemical shift of xenon exploring a mesoporous material. In particular, a chemical shift of 91 ppm has been measured in hybrid materials containing nanochannels with a similar cross section of about 4 nm.[20] On decreasing the temperature from 354 to 143 K there is a downfield shift due to the increased xenon adsorption on the walls of the internal surfaces, where xenon resides for a longer time than the residence time in the mesopore space. At temperatures below 210 K, xenon condensation on the external surfaces contributes considerably to this downfield shift of the resonances and causes the increase in line width. Thus, for the description of the mesopores, the spectra at temperatures above 210 K, that show narrow and symmetrical signals, must be taken into account. The dependence of chemical shift on temperature is depicted in Figure 8b. In the approximation of fast exchange and weak adsorption of xenon, the chemical shift is explained by a model of fast exchange between adsorbed xenon on the internal surface and xenon diffusing in the free space of the channels. In the latter case, xenon experiences the same interactions as in the gas phase and therefore resonates at 0 ppm, while the chemical shift of xenon on the internal surface δ_s is not known *a priori*. The dependence of chemical shift on temperature follows the equation

$$\delta = \delta_s\left(1 + \frac{V}{SK_0R\sqrt{T}}\,e^{-\Delta H_{ads}/RT}\right)^{-1}$$

where V and S correspond to the volume and surface area of mesopores, ΔH is the adsorption enthalpy and K_0 is the pre-exponent of Henry's constant.[21] Exploiting the S and V values from nitrogen adsorption (780.34 $m^2\ g^{-1}$ and 0.78 $cm^3\ g^{-1}$, respectively), the nonlinear least-squares fitting of the chemical shift vs temperature gives the values ΔH_{ads} of 13.9 kJ mol^{-1}, δ_s of 119.6 ppm, and K_0 of 1.094×10^{-11}(mol·$K^{1/2}$)/(Torr·m^2). The Henry's constant measured independently by xenon adsorption isotherm is in agreement with the value of K_0 reported above.

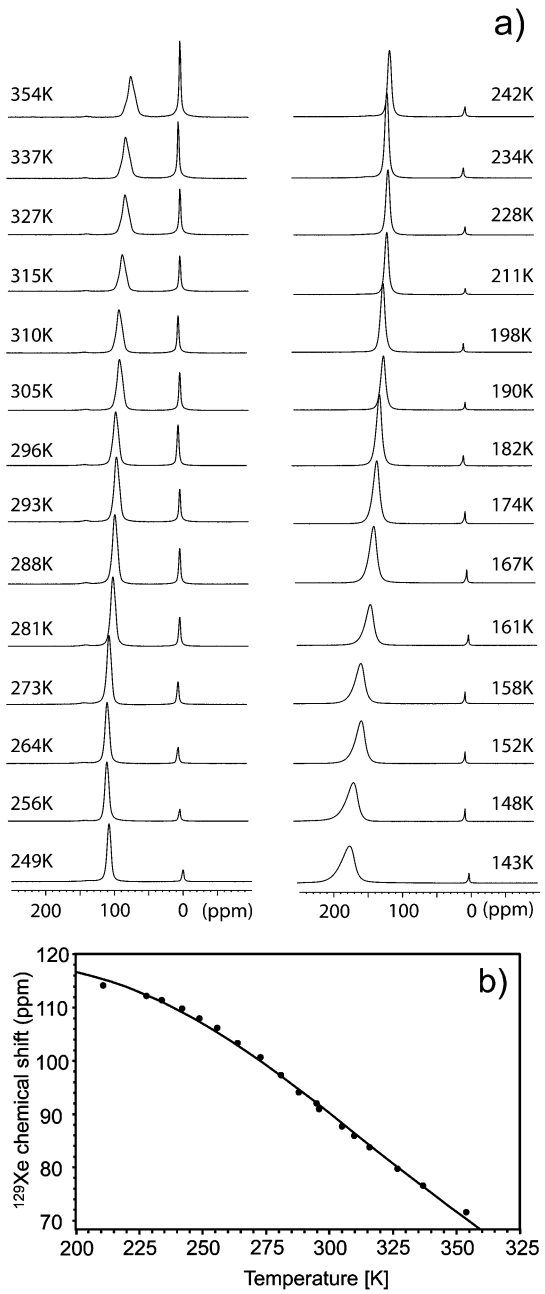

Figure 8. (a) Continuous-flow hyperpolarized ^{129}Xe NMR spectra of the *p*-phenylenesilica at variable temperatures: the peak at 0 ppm is due to the free xenon and the downfield peak to the xenon exploring the nanochannels. (b) Plot of the chemical shifts of xenon diffused to the nanochannels of *p*-phenylenesilica as function of temperature. The chemical shifts vs temperature are fitted by the nonlinear least-squares refinement procedure following the function reported in the text.

(20) (a) Terskik, V. V.; Moudrakvski, I. L.; Breeze, S. R.; Lang, S.; Ratcliffe, C. I.; Ripmeester, J. A.; Sayari, A. *Langmuir* **2002**, *18*, 5653−5656. (b) Nossov, A.; Haddad, E.; Guenneau, F.; Di Renzo, F.; Famula, F.; Gédéon, A. *J. Phys. Chem. B* **2003**, *107*, 12456−12460.

(21) (a) Terskik, V. V.; Mudrakovski, I. L.; Mastikhin, V. M. *J. Chem. Soc. Farady Trans.* **1993**, *89*, 4239−4243. (b) Huang, S.-J.; Huang, C.-H.; Chen, W.-H.; Sun, X.; Zeng, X.; Lee, H.-K.; Ripmeester, J. A.; Mou, C.-Y.; Liu, S.-B. *J. Phys. Chem. B* **2005**, *109*, 681−684.

The consistency of the parameters from HP ^{129}Xe NMR, as well as the nitrogen and xenon adsorption isotherms, allows us to conclude that the cylindrical model can be applied to the mesopores. The absence of hysteresis in the nitrogen adsorption isotherm indicates that there were no micropores and defects in the sample. In addition, the HP Xe measurements enable to determine an adsorption ΔH value of 13.9 kJ mol^{-1}, indicating a physisorption phenomenon. The chemical shift of xenon probing the surfaces $\delta_s = 119.6$ ppm is close to that recorded for amorphous organosilica with similarly sized channels and organic moieties partly exposed to the channels.[20a] In our ordered mesoporous materials, the coverage of the internal surface by aromatic layers is 60%. Larger values of chemical shift are observed only when internal silica surfaces are completely lined with long alkyl chains and high degrees of coverage with organic moieties are reached.[21]

The exchange dynamics of xenon between the confined space and the gas phase is an additional point of interest. In the hyperpolarized ^{129}Xe NMR spectra, the two signals of the free gas and the xenon exploring the nanochannels resonate at 5600 Hz apart, indicating that the exchange time between the two states, if any exchange occurs, must be longer than 0.2 ms (the time τ can be determined in the fast exchange limit by the formula $\tau \cdot \Delta\omega \leq 1$, where $\Delta\omega$ is the difference of the xenon chemical shifts). However, a massive exchange must occur within 200 ms, as a $\pi/2$ pulse generates an intense signal of hyperpolarized xenon diffused in the porous material 200 ms from the cancellation of the magnetization.[22] To evaluate the exchange times on intermediate scales, the targeted experiment of hyperpolarized ^{129}Xe 2D exchange NMR could be employed.[14,23] The experiment was performed at room temperature, with mixing times ranging from 1 to 30 ms (Figure 9).

At 1 ms of exchange time virtually no cross-peaks are present, but starting from a mixing time of 2 ms the intensity of the cross-peaks increases constantly, and becomes substantial in the order of tens of milliseconds. Figure 9b shows the traces at 0 ppm of the spectra, highlighting the comparison of the cross-peak and the diagonal peak intensities. In Figure 9c the normalized intensity of the cross-peaks at increasing mixing times can be seen. The 2D experiments straightforwardly demonstrate that the mesopores are open and accessed easily by the gas phase within times of a few milliseconds. In continuous flow conditions we can observe separately the exchange peaks of xenon exploring first the free gas and then the confined space (diffusing in) as well as xenon diffusing out.[24] In the present case, the intensities of both diffusing-in and -out cross-peaks are essentially balanced, guaranteeing that the relaxation times are sufficiently long to allow the detection of the reversible pathway of xenon within the mesopores and the bulk gas.

Adsorption Measurements. The permanent mesoporosity and the high surface area of the ordered organosilica was exploited to test the adsorption properties of several vapors and gases. Benzene, hexafluorobenzene, and cyclohexane adsorptions show a type-IV isotherm, typical of mesoporous materials

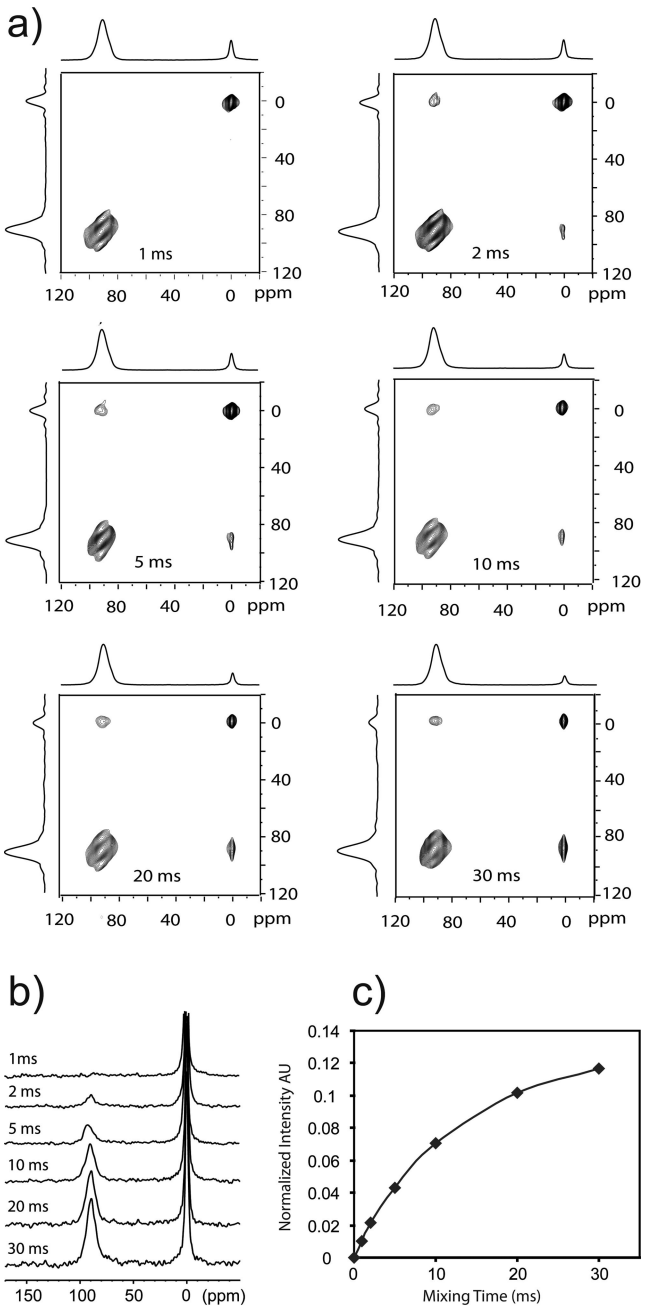

Figure 9. (a) 2D exchange hyperpolarized ^{129}Xe NMR experiments under continuous flow at variable mixing times. (b) ^{129}Xe NMR traces of the 2D exchange spectra at 0 ppm. (c) Cross-peak intensities normalized over the diagonal peaks vs mixing times.

with good affinity for the adsorbates (Figure 10). No hysteresis was present in the desorption branches, as was also evident from the nitrogen isotherms (Supporting Information), indicating the absence of bottlenecks along the channels explored by these vapors.[25] From the benzene isotherm, a capacity of 101.16 cm^3 g^{-1} was measured at p/p_0 of 0.73, hexafluorobenzene isotherm behavior is similar to that of benzene, indicating that the fluorine substitution on the aromatic rings does not notably change the interactions with the hybrid inorganic−organic walls of the nanochannels. This comparison gives some insight into the nature of the channel walls and the geometry of the organic

(22) Meersmann, T.; Logan, J. W.; Simonutti, R.; Caldarelli, S.; Comotti, A.; Sozzani, P.; Kaiser, L. G.; Pines, A. *J. Phys. Chem. A* **2000**, *104*, 11665−11670.
(23) (a) Tallavaara, P.; Jokisaari, J. *Phys. Chem. Chem. Phys.* **2006**, *8*, 4902−4907. (b) Knagge, K.; Smith, J. R.; Smith, L. J.; Buriak, J.; Raftery, D. *Solid State Nucl. Magn. Reson.* **2006**, *29*, 85−89.
(24) (a) Simonutti, R.; Bracco, S.; Comotti, A.; Mauri, M.; Sozzani, P. *Chem. Mater.* **2006**, *18*, 4651−4657. (b) Anala, S.; Pavlovskaya, G. E.; Pichumani, P.; Dieken, T. J.; Olsen, M. D.; Meersmann, T. *J. Am. Chem. Soc.* **2003**, *125*, 13298−13302.
(25) Kruk, M.; Jaroniec, M.; Kim, J. H.; Ryoo, R. *Langmuir* **1999**, *15*, 5279−5284.

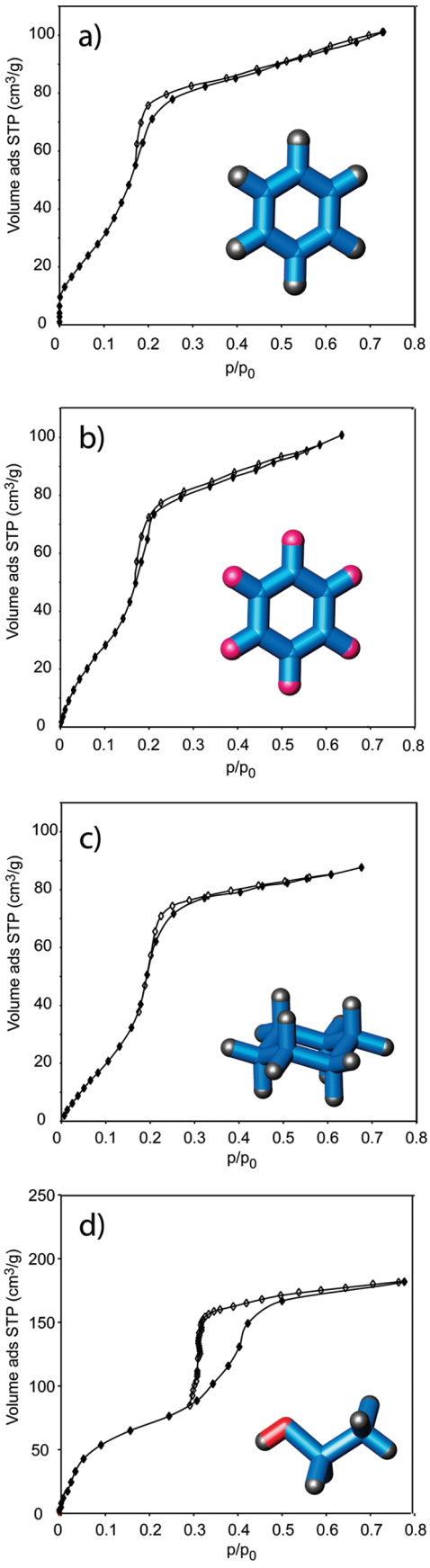

Figure 10. Adsorption isotherms performed at room temperature in *p*-phenylenesilica of (a) benzene, (b) hexafluorobenzene, and (c) cyclohexane. (d) Adsorption isotherm of ethanol at 273 K. Filled symbols denote absorption data.

moieties exposed toward the open cavities. In fact, the wall surface contains *p*-disilylphenylene rings, that are electron-rich systems because of silicon's low electronegativity.[26] In principle, if there were $\pi_{host}\cdots\pi_{guest}$ interactions with the aromatic walls, at low pressure one would expect a steeper adsorption isotherm slope of the hexafluorobenzene because of its electrodeficient ring (the binding energy of parallel stacked hexafluorobenzene−benzene dimers at a distance of 3.6 Å is 20 kJ mol^{-1}).[27] Indeed, such a $\pi_{host}\cdots\pi_{guest}$ interaction is not feasible as the planes of the *p*-disilylphenylene rings cannot face the nanochannels because of steric hindrance with the neighboring rings, and their π_{host}-system is buried within the walls. The 4.35 Å center-to-center distance between the aromatic rings in the host walls, measured by X-ray diffraction, is too short to be compatible with the π_{host} electron clouds facing the channels. In addition, we tested the adsorption properties of the material toward a saturated molecule containing the same number of carbons as cyclohexane. In spite of its aliphatic nature, the amount of moles adsorbed (3.89 mmol g^{-1}) is comparable to that of benzene, indicating that the absence of the polarizable π-system in cyclohexane does not markedly affect the overall trend of the adsorption. However, the initial slope of the curve at $p/p_0 < 0.05$ is less steep than that of benzene and hexafluorobenzene, suggesting that, at low surface coverage, the interactions of the adsorbed aromatic guests with the walls are favored by their polarizable π_{guest}-system due to the occurrence of $CH_{host}\cdots\pi_{guest}$ and $OH_{host}\cdots\pi_{guest}$ weak interactions.[28]

The isotherm of ethanol adsorption in the mesoporous hybrid silica shows a type-IV curve exhibiting a hysteresis loop, as already observed in MCM41.[29] The matrix can store up to 8.7 mmol g^{-1} (40.2% by weight) of the polar molecule at 273 K and 3 mmol g^{-1} already at the low pressure of $p/p_0 = 0.1$.

Methane, at 195 K and a moderate pressure of 700 Torr, could be stored for values of up to 56 cm^3 g^{-1} (STP), and the isotherm curve indicates that saturation has still not been reached under these conditions. This methane uptake corresponds to 4% by weight, and exceeds the uptake of most inorganic zeolites containing 1D channels (about 2.5%).[30a,b] The system appears to be competitive, especially at low pressures. In fact, MCM41 adsorbs a comparable amount of natural gas at room temperature (49 cm^{3}g^{-1} STP), but at the drastic pressure of 35 bar.[30c,d] Carbon dioxide adsorption at 195 K reaches the remarkable value of 20 mmol g^{-1} corresponding to 88% by weight. Taking into account the density of liquid CO_2 at its boiling point, the available pore volume is calculated to be 0.85 mL g^{-1} that, compared to the N_2 adsorption at 77 K, demonstrates a virtual 100% filling of the nanochannels. The type-IV isotherm shows no hysteresis over the full pressure range, indicating easy accessibility to the nanochannels and efficient reversibility of the gas uptake. The high adsorption values prompted us to

(26) Silicon and hydrogen are electron donors with comparable electronegativity values of 1.8 and 2.1.
(27) (a) Meyer, E. A.; Castellano, R. K.; Diederich, F. *Angew. Chem., Int. Ed.* **2003**, *42*, 1210−1250. (b) Bacchi, S.; Benaglia, M.; Cozzi, F.; Demartin, F.; Filippini, G.; Gavezzotti, A. *Chem. Eur. J.* **2006**, *12*, 3538−3546. (c) Williams, J. H. *Acc. Chem. Res.* **1993**, *26*, 593−598. (d) Patrick, C. R.; Prosser, G. S. *Nature* **1960**, *187*, 1021.
(28) (a) Nishio, M.; Hirota, M.; Umezawa, Y. *The CH/π Interaction. Evidence, Nature and Consequences*; Wiley: New York, 1998. (b) Desiraju, G. R. *Acc. Chem. Res.* **2002**, *35*, 565−573.
(29) Branton, P. J.; Hall, P. G.; Sing, K. S. W. *Adsorption* **1995**, *1*, 77−82.
(30) (a) Breck, D. W. *Zeolite Molecular Sieves. Structure, Chemistry and Use*; Wiley: New York, 1974; pp 593−699. (b) Choudhart, V. R.; Mayadevi, S. *Zeolites* **1996**, *17*, 501−507. (c) He, Y.; Seaton, N. A. *Langmuir* **2006**, *22*, 1150−1155. (d) Yun, J.-H.; Duren, T.; Keil, F. J.; Seaton, N. A. *Langmuir* **2002**, *18*, 2693−2701.

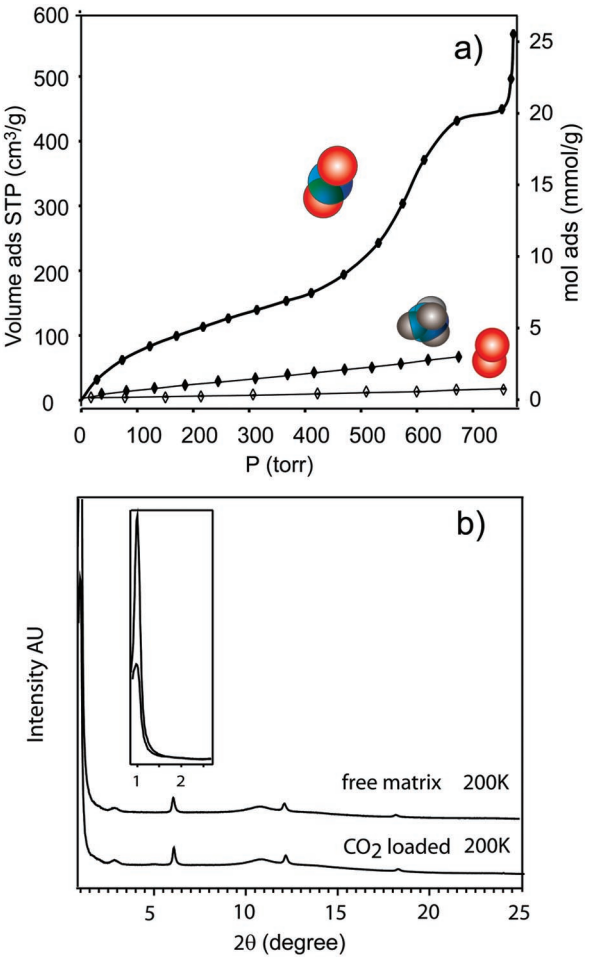

Figure 11. (a) Adsorption isotherms of carbon dioxide and methane at 195 K and oxygen at 273 K in mesoporous *p*-phenylenesilica. (b) Synchrotron X-ray diffraction patterns at 200 K of the matrix with empty channels and loaded with CO_2 at 1 atm. The free sample was heated at 400 K and 10^{-2} Torr for 2 h and then cooled at 200 K under vacuum. In the insert the region at low 2θ angles from 0.8° to 2.8° is enlarged. The weak peak at 2θ of 4.6° is due to the polyimide film to avoid the formation of ice on the capillary.

perform synchrotron radiation X-ray diffraction experiments on the organosilica at 200 K under 1 atm CO_2 loading, as presented in Figure 11. The high electron density due to the CO_2 trapped in the nanochannels reduces the contrast with the channel walls, and accordingly, the signal intensity of the mesoscale periodicity at *d*-spacing of 45.7 Å is reduced to 45% of its original value. This is strikingly evident when the powder pattern of the CO_2-filled mesostructure is compared with that of the empty pore matrix. The molecular-scale order is clearly retained. This is a rare observation of carbon dioxide confined to a mesoporous material by synchrotron radiation diffraction experiments. The adsorption isotherms performed at different temperatures revealed an interaction energy of 19 kJ mol^{-1}, falling in the range of physisorption. The high storage capacity of ordered organosilica for an environmentally important gas like CO_2 has been demonstrated here, and is comparable with that of MCM-41 (18−21 mmol g^{-1}) under the same pressure and temperature conditions.[31] The amount of adsorbed oxygen at 273 K and 700 Torr is 1.3% by weight, and hydrogen adsorption under the same conditions is negligible,[32] suggesting the selective adsorption of carbon dioxide from mixtures with hydrogen and oxygen.[33]

Conclusions

The present work highlights the nanostructure and novel properties of a hybrid mesoporous material with crystalline order in the walls and a periodic, well-organized architecture of siliceous and aromatic layers. For the first time, we have demonstrated, in the hybrid crystalline framework of the *p*-phenylenesilica material, the topological distribution of the organic and inorganic moieties as well as the close spatial relationships between the guest molecules occupying the nanochannels and the host matrix. The application of advanced solid-state NMR techniques has led to the detection of extended interfaces between the crystalline walls and the molecules confined in the nanochannels. Indeed, the multinuclear NMR approach exploiting hydrogen, silicon, and carbon nuclei and 2D experiments with homonuclear Lee−Goldburg decoupling provided the quantitative evaluation of the silica condensed species and the distances between couples of nuclei on the channel walls. In the nanocomposite with the surfactant, we were able to single out the interactions between the polar head groups with siliceous and aromatic layers of the matrix walls by following the magnetization that crosses the organic−inorganic and organic−organic heterogeneous interfaces.

The easy accessibility of the empty nanochannels was demonstrated by hyperpolarized xenon NMR that, due to the high sensitivity of 4 orders of magnitude greater than conventional xenon NMR, provided a unique tool for the exploration of the nanochannel space and surface, collecting information about the channel geometry, adsorption energy, and exchange phenomena. The powerful technique of 2D exchange hyperpolarized xenon experiments determined the xenon exchange dynamics between the confined and the bulk phase as fast as a few milliseconds.

Unprecedented adsorption measurements of vapors of aromatic molecules established the high storage capacity of the material, envisaging its possible use to reduce the toxic content of exhaust emissions. The *p*-phenylene rings on the channel walls expose the CH bonds to interact with the adsorbate guest molecules of benzene and hexafluorobenzene, establishing favorable weak CH···π interactions; π···π interactions are forbidden by the occurring topology of the matrix walls. Ethanol could be loaded up to the high value of 40% by weight.

Gases important for environmental and energetic reasons, such as methane and carbon dioxide, could be stored efficiently and selectively in the honeycomb structure. The performance of the material is such that carbon dioxide can be captured up to a remarkable value of 90 wt %, making this system one of the most effective for gas storage. Synchrotron X-ray powder diffraction could detect unconventionally in situ the carbon dioxide stored in the nanochannels. The adsorption properties highlight the novel functions of ordered mesoporous hybrid materials; the selective adsorption of carbon dioxide, with respect to hydrogen and other gases, supports the utility of this

(31) Morishige, K.; Fujii, H.; Uga, M.; Kinukawa, D. *Langmuir* **1997**, *13*, 3494−3498.

(32) (a) The adsorption of hydrogen at 77 K and 600 torr is 0.6% by weight: Jung, J. H.; Han, W. S.; Rim, J. A.; Lee, S. J.; Cho, S. J.; Kim, S. Y.; Kang, J. K.; Shinkai, S. *Chem. Lett.* **2006**, *35*, 32−33.

(33) (a) Sozzani, P.; Bracco, S.; Comotti, A.; Ferretti, L.; Simonutti, R. *Angew. Chem., Int. Ed.* **2005**, *44*, 1816−1820. (b) Atwood, J. L.; Barbour, L. J.; Jerga, A. *Angew. Chem., Int. Ed.* **2004**, *43*, 2948−2950.

material as a hydrogen purifier from carbon dioxide contamination, and depresses CO_2 emissions from hydrogen-fueled cells. The material's permanent porosity and high thermal stability, together with its adsorption reversibility, guarantee the feasibility of applying this mesoporous hybrid material to cope with the environmental and energetic problems.

Acknowledgment. We thank E. Ronchi, M. Beretta, and L. Oldrino for their contribution in the synthesis of the materials, M. Merlini for the technical help at the European Synchrotron Radiation Facility in Grenoble, and M. Gemmi for the acquisition of TEM images. R. Simonutti and M. Mauri are gratefully acknowledged for their help in the acquisition of xenon NMR data. We are in debt to Fondazione Cariplo and FIRB for financial support.

Supporting Information Available: Nitrogen adsorption isotherm, thermogravimetric analysis, SEM images, ^{29}Si RAMP-CP MAS spectrum and xenon adsorption isotherms of mesoporous *p*-phenylenesilica; XRD, ^{29}Si and ^{13}C CP MAS spectra, quantitative ^{13}C MAS NMR spectrum, 2D ^{1}H−^{29}Si and ^{1}H−^{13}C heterocorrelated NMR spectra with 3 ms contact time of the d_4-*p*-phenylenesilica; table containing ^{13}C CP MAS and ^{1}H MAS NMR chemical shifts of d_4-*p*-phenylenesilica. This material is available free of charge via the Internet at http://pubs.acs.org.

JA071348Y